Structures, Thermal Properties, and Reactivities of Cationic Rh-cod Complexes in Solid State (cod = 1,5-Cyclooctadiene)

Sumitani, Ryo
Kuwahara, Daisuke
Mochida, Tomoyuki

(Citation)
Inorganic Chemistry,62(5):2169-2180

(Issue Date)
2023-02-06

(Resource Type)
journal article

(Version)
Version of Record

Inorganic Chemistry

pubs.acs.org/IC
Article

Structures, Thermal Properties, and Reactivities of Cationic Rh−cod Complexes in Solid State (cod = 1,5-Cyclooctadiene)

Ryo Sumitani, Daisuke Kuwahara, and Tomoyuki Mochida*

Cite This: *Inorg. Chem.* 2023, 62, 2169−2180
Read Online

ABSTRACT: Cationic rhodium complexes with 1,5-cyclooctadiene (cod) ligands are important organometallic compounds that are useful as precatalysts; however, their solid-state structures and thermal properties have not been adequately investigated. In this study, we synthesized [Rh(cod)L]X (L = cod, C_6H_6, PhMe; X = SbF_6, $(FSO_2)_2N$ (= FSA), CF_3BF_3, $CB_{11}H_{12}$) and investigated their phase behaviors, crystal structures, and reactivities. The phase transitions of these salts result in disordered solid-state structures. Moreover, the structural disorder increases with a decrease in the cation symmetry in the SbF_6 salts; [Rh(cod)(PhMe)]SbF_6 exhibits a rotator phase, and the cations in other salts exhibit a dynamic rotational disorder. In contrast, a lower crystal symmetry with less cation disorder is observed for FSA salts. The thermal stabilities and reactivities of these salts were further investigated. FSA salts with arene ligands produce anion-coordinated complexes upon melting, and SbF_6 salts with arene ligands produce [Rh(cod)L'_2]SbF_6 (L′ = MeCN and SMe_2) via an in situ single-crystal-to-single-crystal ligand-exchange reaction.

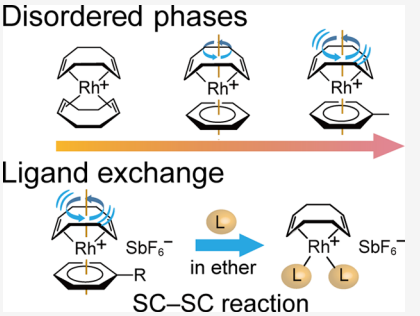

INTRODUCTION

Cationic rhodium complexes with diene ligands such as 1,5-cyclooctadiene (cod) are important organometallic species that are useful for various catalytic applications, such as the hydrogenation of alkynes.[1−5] Among them, $[Rh(cod)_2]^+$ serves as a precatalyst and can be used for the in situ generation of catalysts via ligand exchange. The catalytic activities of Rh−cod complexes are affected by the thermodynamics and kinetics of their ligand exchange reactions.[6] In recent years, research on solid-state organic reactions has become increasingly important.[7] Although solid-state properties of Rh−cod complexes are important for exploring solid-state organometallic reaction chemistry, this aspect has received little attention.[8] In contrast, extensive solid-state research has been conducted on the chemistry of sandwich compounds such as ferrocene, cobaltocene, and their derivatives.[9,10] Salts of cationic sandwich complexes, such as $[Fe(C_5H_5)_2]PF_6$, typically exhibit an ionic plastic crystal (IPC) phase because of the spherical shape of their cations.[11−16] The constituent molecules undergo fast reorientation or rotation in the IPC phase, resulting in high crystal symmetry and ionic conductivity.[17−29] Therefore, we hypothesized that salts of cationic Rh-cod complexes also exhibit an IPC or rotator phase. Molecules in the rotator phase typically rotate along the molecular long axis.[30−33] Furthermore, $[Rh(cod)_2]^+$ and its derivatives readily undergo ligand exchange reactions in solution,[34] although their solid-state reactivity has not been investigated. Crystalline phase reactions require structural flexibility or reaction cavities; hence, IPC or rotator phases may provide a suitable reaction medium for ligand exchange reactions.

The present study reports the structures, thermal properties, and reactivities of [Rh(cod)L]X (L = cod ([**1**]X), C_6H_6 ([**2**]X), PhMe ([**3**]X), X = SbF_6, $(FSO_2)_2N$ (= FSA), CF_3BF_3, $CB_{11}H_{12}$), and $[Ir(cod)_2]SbF_6$ ([**1′**]SbF_6) in the solid state (Figure 1). Among these, [**1**]SbF_6,[35] [**1′**]SbF_6,[36] and [**2**]SbF_6[5] are known compounds. Most of the anions are nearly spherical and are often used as components of IPCs, whereas the FSA anion (= $(FSO_2)_2N^-$) is typically used for ionic liquids.[37,38] First, we discuss the phase transitions and thermal decomposition behavior of [**1**]X, [**2**]X, and [**3**]X (X = SbF_6, FSA). [**1′**]SbF_6 and Rh−cod complexes with CF_3BF_3 and $CB_{11}H_{12}$ anions were also studied. These salts exhibit phase transitions that produce disordered structures in the solid state, of which [**3**]SbF_6 exhibits a rotator phase at room temperature. The melting behavior of the FSA salts was investigated in detail. In addition, the cation dynamics of the SbF_6 salts were investigated by solid-state NMR spectroscopy. Finally, we investigated the reactivity of SbF_6 salts with arene ligands and observed that in situ ligand exchange occurs in ether via a single-crystal-to-single-crystal (SC−SC) reaction.

Received: November 2, 2022
Published: January 26, 2023

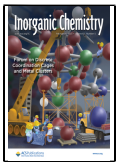

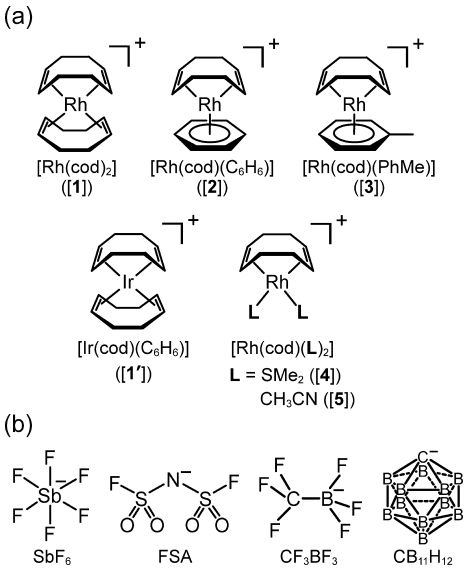

Figure 1. Structural formulae of (a) cations and (b) anions used in this study.

RESULTS AND DISCUSSION

Phase Behaviors. The phase behavior of [**1**]X−[**3**]X (X = SbF_6, FSA, CF_3BF_3, and $CB_{11}H_{12}$) was investigated using differential scanning calorimetry (DSC). The phase sequences and DSC curves of the salts are shown in Figures 2 and S1, respectively. All the salts exhibit solid phase transitions, and the lowest temperature phase in each salt is designated as phase I. These salts decompose without melting at high temperatures, except for [**1**]FSA and [**2**]FSA, which melt at approximately 360 K.

The phase sequences of the SbF_6 salts are shown in Figure 2a. [**1**]SbF_6 exhibits a phase transition at 329.9 K (ΔS = 19.6 J mol^{-1} K^{-1}), and the corresponding Ir complex ([**1′**]SbF_6) exhibits a phase transition at almost the same temperature (327.4 K). [**2**]SbF_6 exhibits four phase transitions, and the sum of its transition entropies (ΔS_{total} = 16.6 J mol^{-1} K^{-1}) is comparable to that of [**1**]SbF_6. [**3**]SbF_6 exhibits a phase transition from phase I to II, which is a rotator phase (see below), at 271.6 K (ΔS = 33.7 J mol^{-1} K^{-1}). This transition entropy is quite large and comparable to those of sandwich complexes from an anisotropic crystalline phase to a plastic phase (e.g., [Ru(Cp)(PhMe)]PF_6, ΔS = 29.0 J mol^{-1} K^{-1} [11,14]). The transition from phase II to III at 452.3 K (ΔS = 6.8 J mol^{-1} K^{-1}) is a transition between rotator phases; birefringence was observed in both phases under a polarizing optical microscope, indicating their anisotropic crystal structures (Figure S2).

The phase sequences of the FSA salts are shown in Figure 2b. [**1**]FSA undergoes a phase transition at 307.4 K (ΔS = 30.6 J mol^{-1} K^{-1}). [**2**]FSA and [**3**]FSA exhibit phase transitions at 358.7 and 350.3 K, followed by melting at 369.2 and 363.3 K, respectively. The details of the melting phenomenon are discussed in the next section.

The phase sequences of salts with other anions (X = CF_3BF_3 and $CB_{11}H_{12}$) are shown in Figure 2c. [**1**]CF_3BF_3 and [**3**]CF_3BF_3 exhibit two and six phase transitions, respectively, which occur at considerably lower temperatures than those of the other salts, probably because the CF_3BF_3 anion facilitates disorder.[16] [**1**]CF_3BF_3 undergoes a phase transition from phase I to II at 212.6 K (ΔS = 16.8 J mol^{-1} K^{-1}), whereas

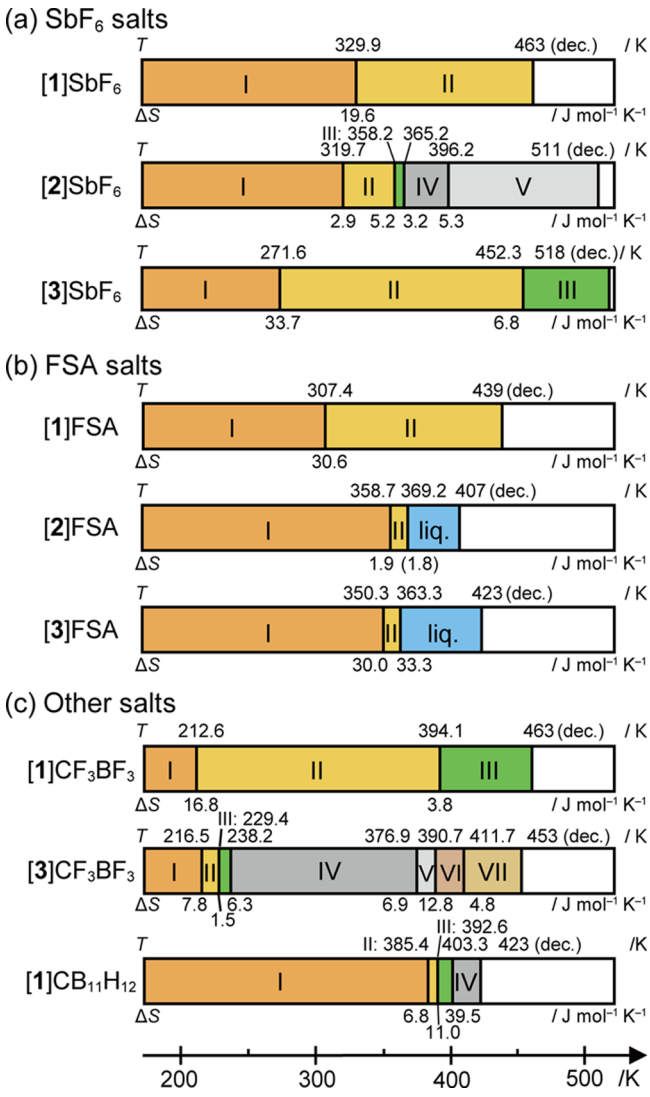

Figure 2. Phase sequences of [**1**]X−[**3**]X with (a) SbF_6, (b) FSA, and (c) other anions. The phase transition temperature (K) and transition entropy (J mol^{-1} K^{-1}) of each phase transition are shown above and below the bar charts, respectively. The liquid phases of [**2**]FSA and [**3**]FSA contain thermal reaction products (see text).

[**3**]CF_3BF_3 undergoes three successive phase transitions at approximately 230 K and the sum of the transition entropies (ΔS_{sum} = 15.6 J mol^{-1} K^{-1}) is comparable to that of [**1**]CF_3BF_3. [**1**]$CB_{11}H_{12}$, which contains the carborane anion, exhibits three phase transitions above 385.4 K, probably because of the large anion volume, facilitating its molecular rotation only at high temperatures. Other salts such as [**2**]CF_3BF_3 could not be synthesized because ligand exchange from [**1**]CF_3BF_3 did not occur.[34] Similarly, [**2**]$CB_{11}H_{12}$ and [**3**]$CB_{11}H_{12}$ were not obtained, probably because of anion coordination.[39]

Most salts showed successive phase transitions as a result of successive order−disorder rearrangements of cations and anions (see below), similar to the salts of sandwich complexes,[13] although none of the current salts exhibits an IPC phase; optical birefringence was observed for all phases. This is probably because of the elongated cation shapes compared to that of $[M(Cp)_2]^+$, which hinders isotropic rotation. However, the salts exhibit dynamic phases, including rotator phases, as described below.

https://doi.org/10.1021/acs.inorgchem.2c03865
Inorg. Chem. 2023, 62, 2169−2180

Melting Behaviors of FSA Salts. We investigated the melting behaviors of [**2**]FSA and [**3**]FSA in detail. Interestingly, ligand exchange reactions occurred after melting to form anion-coordinated complexes (Figure 3a).

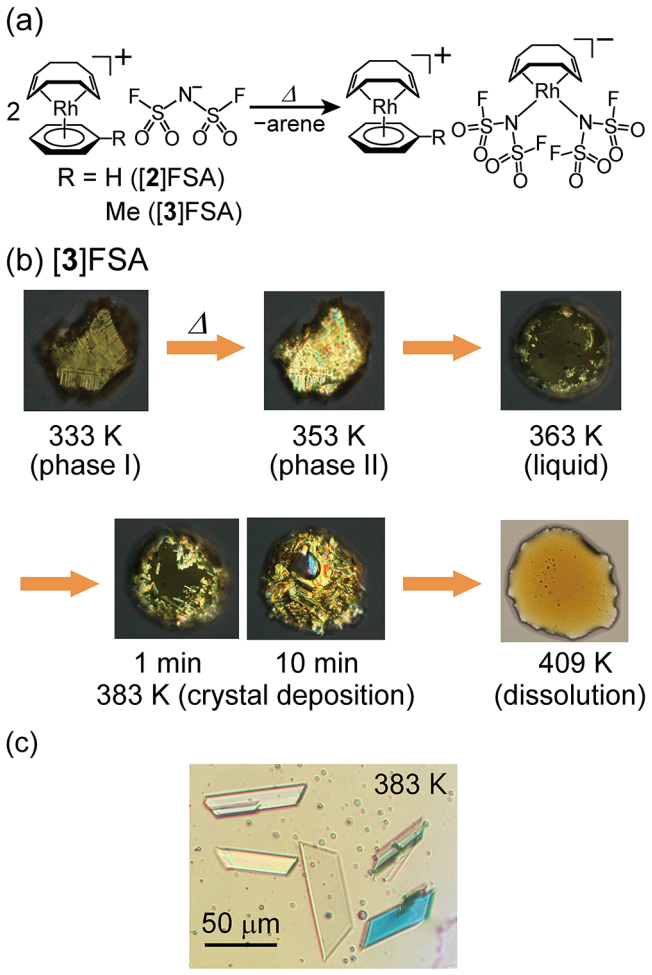

Figure 3. (a) Ligand exchange reaction of [**2**]FSA and [**3**]FSA that occurred upon their melting. (b) POM images of [**3**]FSA taken during heating. (c) Microscopic image of the crystals grown in the melt of [**3**]FSA taken under polarized light, after breaking up an aggregate using a needle.

Polarizing optical microscopy (POM) images of the melting behavior of the [**3**]FSA are shown in Figure 3b. This salt melts at 363 K, after which the deposition of crystals in the melt occurs within 10 min when the liquid is maintained at 383 K, and the crystals dissolve upon further heating to 409 K. [**2**]FSA exhibits a similar behavior by melting at 369 K, followed by crystal deposition (Figure S3). The entropy change observed by DSC at the melting point was small for this salt (Figure 2) because melting overlapped with the exotherm from the ligand exchange reaction.

X-ray structural analysis of the crystal formed upon melting [**3**]FSA at 388 K showed the structure to be [**3**][Rh(cod)-(FSA)$_2$]. The compound contains an anionic complex with two FSA anions coordinated to the metal center via N atoms (Figure 3a, right), indicating that the arene ligands of every second cation are exchanged for anions. The molecular structure of this anion is shown in Figure S4. However, we do not provide a detailed structural discussion because of its low data quality ($R_1[I > 2\sigma(I)] = 14.4\%$). Structural analysis of the reaction product of [**2**]FSA was not possible.

Although several group-11 metal complexes are known to be coordinated via the N atom of FSA or Tf_2N (= $(CF_3SO_2)_2N^-$),[40−43] very few have been studied such as platinum-group metal complexes.[44] A related phenomenon is the formation of the anion-coordinated complex [Ir(cod)-(OTf)] (OTf = $CF_3SO_3^-$) as an intermediate in the ligand exchange reaction of [Ir(cod)(*p*-xylene)]OTf in solution.[45] The formation of anion-coordinated complexes in the liquid phase observedin this study is consistent with this phenomenon.

Thermal Decomposition Behaviors. The thermal stability of [**1**]X−[**3**]X (X = SbF_6, FSA) was investigated by thermogravimetric (TG) measurements. FSA salts decompose at lower temperatures than SbF_6 salts. The TG curves were measured at a scan rate of 3 K min^{-1} under a nitrogen atmosphere, as shown in Figures 4 and S5. The decomposition temperatures (T_{dec} = 3 wt % weight loss temperature) determined from the curves are listed in Table 1, together with those of the related salts.

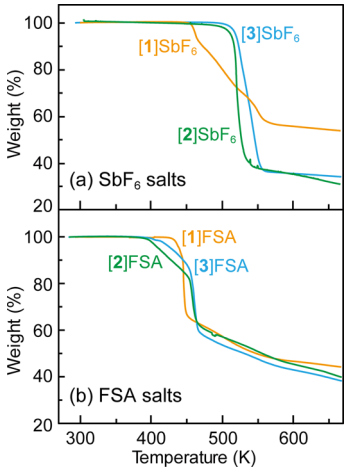

Figure 4. TG traces of (a) SbF_6 and (b) FSA salts measured at a scan rate of 3 K min^{-1} in a nitrogen atmosphere.

The TG curves of the SbF_6 salts are shown in Figure 4a. [**1**]SbF_6 decomposes at 463 K and exhibits a weight loss of approximately 36 wt % up to 548 K owing to the loss of two cod ligands (calculated value: −39 wt %). The decomposition

Table 1. Decomposition Temperatures (T_{dec}) of Salts Containing Rh−cod Complexes (K)[a]

salt	T_{dec}	salt	T_{dec}
[**1**]SbF_6	463	[**1**]$CB_{11}H_{12}$[c]	423
[**1′**]SbF_6	421	[**1**]CF_3BF_3[b]	463
[**2**]SbF_6	511	[**1**]BAr^F_4[b,d]	437
[**3**]SbF_6	518	[**1**]BF_4	454
[**1**]FSA	439	[**3**]CF_3BF_3[c]	453
[**2**]FSA	407	[**3**]BF_4[b,e]	447
[**3**]FSA	423	[**4**]SbF_6	433
		[**5**]SbF_6	441

[a]Determined by TG measurement (−3 wt %) unless otherwise specified. [b]Determined by visual inspection. [c]Determined by DSC measurement (peak-top temperature). [d]Ref 46. [e]Ref 34 (described as a melting point).

https://doi.org/10.1021/acs.inorgchem.2c03865
Inorg. Chem. 2023, 62, 2169−2180

temperature is similar to those of [**1**]BF_4 (454 K, determined by TG, Figure S5c) and [**1**]$BAr^F{}_4$ (T_{dec} = 437 K, $BAr^F{}_4$ = tetrakis((3,5-trifluoromethyl)phenyl)borate),[46] indicating that the cation is responsible for the decomposition. The arene-coordinated complexes, [**2**]SbF_6 and [**3**]SbF_6, exhibit considerably higher decomposition temperatures of 511 and 518 K, respectively; [**3**]SbF_6 is more stable owing to the electron-donating substituent in the ligand. Each salt exhibits a weight loss of approximately 65 wt % in one step, which may be ascribed to the loss of cod, arene ligand (calculated value: −37 wt %), and some SbF_5 formed by partial decomposition of the anion.

The TG curves of the FSA salts are shown in Figure 4b. The decomposition temperature of [**1**]FSA is 439 K, approximately 20 K lower than that of [**1**]SbF_6. The weight loss of approximately 34 wt % occurs in one step owing to the loss of two cod ligands (calculated value: −37 wt %). In contrast, the decomposition temperatures of [**2**]FSA and [**3**]FSA are 407 and 423 K, respectively, approximately 100 K lower than those of the corresponding SbF_6 salts owing to ligand exchange reactions that occur upon melting, as described above. Namely, the decomposition is ascribed to the coordination ability of the anions, which leads to ligand dissociation. These salts exhibit weight losses of 18 and 12 wt %, respectively, within a temperature range of 390−450 K, which corresponds to the loss of arene ligands (calculated values: −16 and −19 wt %, respectively). [**1**]$CB_{11}H_{12}$ exhibits a similar decomposition temperature (423 K), which is consistent with the coordination ability of the carborane anion.[39]

In addition, the decomposition behavior of the Ir complex [**1′**]SbF_6 was investigated. The lower decomposition temperature (T_{dec} = 421 K) of this salt compared to that of [**1**]SbF_6 (T_{dec} = 463 K) indicates weaker coordination bonding. A similar tendency has been reported for the melting points of BF_4 salts ([**1′**]BF_4:413−418 K, [**1**]BF_4:479−481 K),[47] which are probably accompanied by decomposition.

General Features of the Crystal Structures. The crystal structures of phase I of the salts were determined, except for [**3**]SbF_6 and [**3**]CF_3BF_3, and the structural changes from phase I to II were crystallographically elucidated for most salts (Figure 5). Their structural features are dependent on the anion, cation, and radius ratio, as summarized in this section. In higher-temperature phases, the structural disorder is enhanced to a larger extent when the transition entropy is large.

A correlation was observed between molecular and crystal structures. In phase I, the crystal system of the FSA salts is monoclinic, reflecting low anion symmetry, whereas those of the other salts (X = SbF_6, CF_3BF_3, and $CB_{11}H_{12}$) are orthorhombic, except for [**1**]SbF_6. The cations and anions are arranged alternately in all the salts, where the number of cations surrounding the anions (coordination number)[48] is eight for [**1**]$CB_{11}H_{12}$, seven for [**2**]SbF_6, and six for all others in phase I. The cation-to-anion radius ratio ρ, calculated from the van der Waals volumes of the molecules, is 0.87 for $CB_{11}H_{12}$ salts, whereas it is 0.71, 0.68, and 0.65 for FSA, CF_3BF_3, and SbF_6 salts, respectively. Thus, with the exception of [**2**]SbF_6, the results are consistent with the radius ratio rule for ionic crystals,[49] which determines the six-coordinated ($0.41 < \rho < 0.73$) or eight-coordinated ($0.73 < \rho$) structures. Interestingly, the coordination number of [**1**]FSA, whose radius ratio is close to the boundary, changed from six in phase I to eight in phase II, owing to an increase in the effective volume caused by anion disorder in phase II.

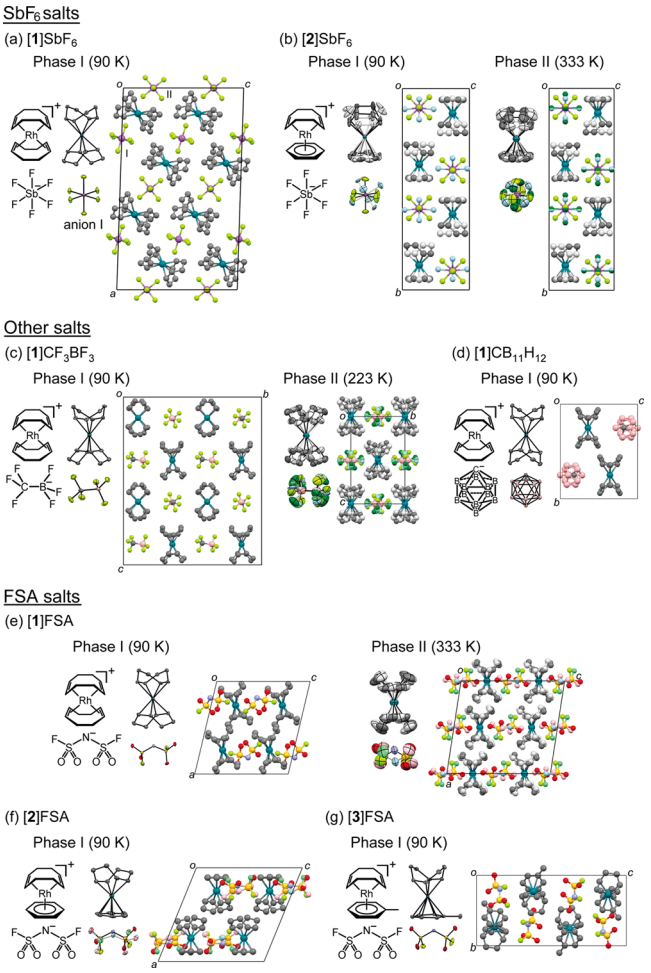

Figure 5. Molecular structures (left, ORTEP drawing, 50% probability level) and packing diagrams (right) of [**1**]X−[**3**]X. (a,b) SbF_6 salts, (c,d) other salts, and (e−g) FSA salts. Less occupied parts of disordered groups are shown in a lighter color.

Although phase I is an ordered phase for a majority of the salts, structural disorder of this phase increases as the cation symmetry decreases in the order [**1**]X, [**2**]X, and [**3**]X. Both cations and anions are ordered in [**1**]X (X = SbF_6, CF_3BF_3, and $CB_{11}H_{12}$) with high packing coefficients (72.8−73.2%), and both exhibit disorder in [**2**]SbF_6, and are even more extensively disordered in [**3**]X (X = SbF_6 and CF_3BF_3). The FSA salts exhibit less disorder. In each salt, the structural disorder increases, and the crystal symmetry tends to be higher for higher-temperature phases.

Cation disorder is typically a twofold rotational disorder around the long axis, as seen in [**2**]SbF_6 (phases I and II), [**1**]FSA (phase II), and [**1**]CF_3BF_3 (phase II), reflecting the elongated cation shape (Figure 5). Cation structures in other high-temperature phases could not be determined because of extensive disorder. Ordered cations were found in phase I of [**1**]CF_3BF_3, [**1**]$CB_{11}H_{12}$, and [**1**]FSA−[**3**]FSA, with geometries almost identical to those of [Rh(cod)$_2$]X (X = BF_4, OTf)[50,51] and [Rh(cod)(arene)]SbF_6 (arene = hexamethylbenzene, 1,4-dimethylnaphthalene, etc.).[5]

The structure of each salt is discussed in detail in the following sections.

https://doi.org/10.1021/acs.inorgchem.2c03865
Inorg. Chem. 2023, 62, 2169−2180

Crystal Structures of SbF_6 Salts. The structural disorder becomes more extensive with a decrease in cation symmetry from **1** to **3**. The structure of [**1**]SbF_6 at 90 K (phase I), shown in Figure 5a, has an ordered phase with a coordination number of six. The structure of phase II could not be fully refined because of extensive rotational disorder. The space groups of phases I and II are monoclinic $C2/c$ and orthorhombic A, respectively, with $Z = 8$ (Table S1), where molecular rotation leads to a higher symmetry in phase II. The corresponding Ir complex [**1′**]SbF_6 is isomorphous, and its unit cell volume is identical to that of [**1**]SbF_6 within the standard deviation (Figure S6). Their molecular structures are almost identical, with $M-C_{(cod)}$ distances of 2.220(2)−2.269(2) Å (M = Rh) and 2.196(7)−2.254(7) Å (M = Ir).

The structures of [**2**]SbF_6 at 90 K (phase I) and 333 K (phase II) are shown in Figure 5b. The structural changes at the phase transition are small; both phases exhibit the *Cmcm* space group and a coordination number of seven, and their unit cell volumes are almost the same ($Z = 4$). The cations and anions exhibit rotational disorder in both phases. The cod, benzene ligands, and anion were refined as twofold disordered in phase I (occupancy ratios 0.5:0.5, 0.63(2):0.37(2), and 0.654(5):0.346(5)), whereas the anion required refinement of threefold disorder in phase II, with the occupancies becoming more averaged (occupancy ratios 0.5:0.5, 0.56(3):0.44(3), and 0.402(3):0.302(3):0.296(3)). These small structural changes are consistent with the small phase-transition entropy (ΔS = 2.9 J mol K^{-1}). Phase IV (373 K) has the same unit cell and space group as those in phase II; the structure could not be fully refined owing to extensive disorder (Table S2).

The structure of [**3**]SbF_6 could not be determined because of the extensive rotational disorder of the cations in both phases. The powder X-ray diffraction (PXRD) patterns of [**3**]SbF_6 at 90 K (phase I) and 293 K (phase II) are shown in Figure S7a; the pattern at 293 K is considerably simpler, with fewer peaks than that at 90 K. The crystal systems of these phases are orthorhombic P ($Z = 16$) and tetragonal I ($Z = 2$), respectively (Table S7). Molecular rotation (see below) resulted in high crystal symmetry.

Cation Dynamics in SbF_6 Salts. The cation motion in [**1**]SbF_6−[**3**]SbF_6 was investigated using solid-state ^1H and ^2H NMR spectroscopy. As shown in the previous section, X-ray structural analysis revealed that the cation has an ordered structure in [**1**]SbF_6, rotationally disordered structure in [**2**]SbF_6, and extensive disorder in [**3**]SbF_6 at room temperature. To investigate the motion of the cod and arene ligands in the cation independently, salts with benzene-d_6 and toluene-d_8 ligands (d-[**2**]SbF_6 and d-[**3**]SbF_6, respectively) were synthesized and used for NMR measurements.

The motion of the cod ligand was investigated using ^1H NMR spectroscopy. The static ^1H NMR spectra of [**1**]SbF_6, d-[**2**]SbF_6, and d-[**3**]SbF_6 recorded at 299 K are shown in Figure 6a, each displaying the proton signal of the cod ligand. The full-width-at-half-maxima of the peaks for [**1**]SbF_6, d-[**2**]SbF_6, and d-[**3**]SbF_6 are 54.0, 19.3, and 8.9 kHz, and the second moments (M_2) for the signals are 29.1, 3.7, and 0.8 G^2, respectively. The broad signal in [**1**]SbF_6 indicates that the ligand is static, which is consistent with the X-ray structure. The narrow signal in d-[**2**]SbF_6 indicates that the ligand undergoes dynamic reorientation, which demonstrates that the crystallographically observed twofold rotational disorder of cod is dynamic in nature, with the disordered moieties not statically locked in place. A narrow signal was also obtained for d-[**3**]SbF_6 ($M_2 < 1$), indicating that the ligand undergoes extensive motion.[52]

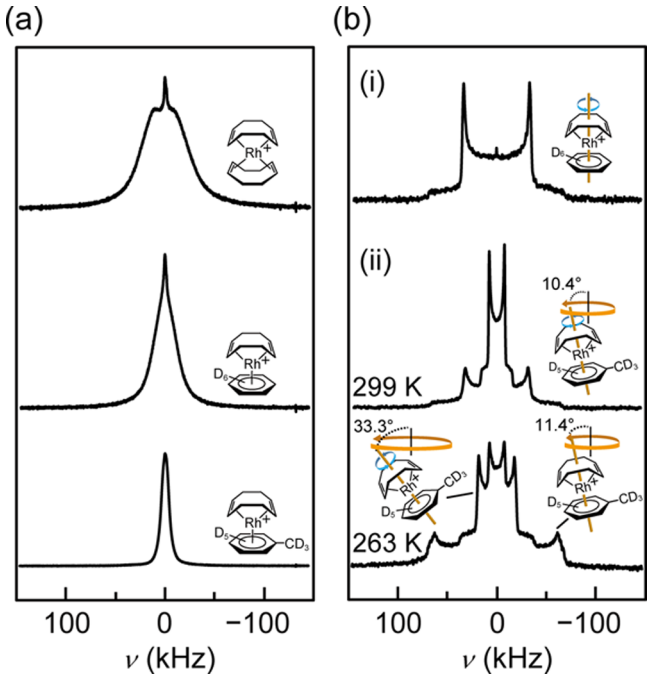

Figure 6. (a) Solid-state static ^1H NMR spectra of [**1**]SbF_6, d-[**2**]SbF_6, and d-[**3**]SbF_6 recorded at 299 K. (b) Solid-state static ^2H NMR spectra of (i) d-[**2**]SbF_6 recorded at 299 K and (ii) d-[**3**]SbF_6 recorded at 299 and 263 K. The molecular motions occurring in each phase are illustrated for each spectrum in (b). The frequency of the center of the resonance line of d-[**3**]SbF_6 was set to 0 Hz for the ^1H NMR spectra, whereas the center of the Pake doublet of [**1**]SbF_6 was set to 0 Hz for the ^2H NMR spectra.

The motions of the deuterated arene ligands in d-[**2**]SbF_6 and d-[**3**]SbF_6 were investigated using ^2H NMR spectroscopy. The static ^2H NMR spectrum of d-[**2**]SbF_6 measured at 296 K is shown in Figure 6b(i), in which the nuclear quadrupole coupling constant (e^2Qq/h) is 88.7 kHz (asymmetry factor η = 0). This value is half that of the static phenyl group (176 kHz),[53] indicating that the benzene ligand undergoes continuous rotational diffusion around the molecular long axis. Therefore, although benzene is rotationally disordered according to X-ray analysis, it rotates faster than the NMR time scale. This phase can also be regarded as rotational in a broader sense.

The solid-state static ^2H NMR spectra of d-[**3**]SbF_6 in phases II (299 K) and I (263 K) are shown in Figure 6b(ii) and consist of two and three components, respectively. In each spectrum, the innermost Pake doublet represents the methyl-D signal, and its small e^2Qq/h value (20.5 kHz in phase II and 20.1 kHz in phase I) indicates continuous rotational motion of the methyl group.[54] The outer Pake doublet at 299 K represents the arene-D signal, and its e^2qQ/h value (84.3 kHz, η = 0) is approximately 4 kHz smaller than that of [**2**]SbF_6. Line shape analysis revealed that the toluene ligand undergoes continuous rotational diffusion around the molecular long axis, accompanied by precessional motion ($\gamma = 10.4°$) of the cation along the molecular long axis, as illustrated in the figure. In contrast, two types of Pake doublets are observed for arene-D at 263 K, indicating the presence of nearly static and dynamic cations. The e^2qQ/h value of the outer signal (165.7 kHz) is approximately 10 kHz smaller than that of the static phenyl

https://doi.org/10.1021/acs.inorgchem.2c03865
Inorg. Chem. 2023, 62, 2169−2180

group, indicating that the ring rotation is nearly frozen, although a slight precessional motion of the cation still exists (γ = 11.4°). The small e^2qQ/h value of the inner signal (48.1 kHz) indicates extensive cation motion, which is analyzed as the continuous rotation of the phenyl ring and large precessional motion of the cation (γ = 33.3°). Alternatively, a larger precessional motion (γ = 44.1°) without molecular rotation would produce the same line shape; however, this seems less plausible.

These analyses reveal the characteristic molecular motion of the Rh−cod cations. The ^{1}H and ^{2}H NMR spectra consistently account for the X-ray structure, and the results suggest the dynamic nature of the twofold disorder of cod observed in other salts. In addition, [**3**]SbF_6 has been demonstrated to exhibit a rotator phase in which the molecules undergo extensive but anisotropic rotation. Considering these results, the room-temperature phase of [**3**]CF_3BF_3 and the high-temperature phases of the other salts are probably rotator phases with extensive molecular motion, similar to [**3**]SbF_6. However, this could not be confirmed experimentally because of the high temperatures or narrow temperature range.

Crystal Structures of CF_3BF_3 and $CB_{11}H_{12}$ Salts. The crystals of [**1**]CF_3BF_3, [**1**]$CB_{11}H_{12}$, and [**3**]CF_3BF_3 belong to an orthorhombic crystal system in phase I, similar to most SbF_6 salts. [**3**]CF_3BF_3 exhibits extensive structural disorder.

The structures of [**1**]CF_3BF_3 determined at 90 K (phase I) and 223 K (phase II) are shown in Figure 5c. Phase I is an ordered phase with space group *Aba*2 (Z = 16). The two pairs of cations and anions are crystallographically independent, and the coordination number is six. The crystal symmetry in phase II is higher (space group *Pnnm*, Z = 2). Phase II is regarded as the averaged structure of phase I, having only one cation−anion pair in the asymmetric unit, with the cation best refined as twofold rotationally disordered (occupancy ratio 0.642(15):0.358(15)). The anion occupies a special position of the twofold rotational axis and mirror plane, with an occupancy ratio of 0.25. As a result, the carbon and boron atoms are refined as twofold rotationally disordered (occupancy ratio 0.5:0.5), occupying almost the same position, and the fluorine atoms are refined as fourfold disordered by rotation (occupancy ratio 0.25). The molecular arrangements in phases I and II are almost identical, with slight shifts in their molecular positions (Figure S8). This structure differs from that of [**1**]OTf (space group $C2/c$ at room temperature, ordered structure),[50] despite the presence of structurally similar anions.

The structure of [**1**]$CB_{11}H_{12}$ at 90 K (phase I) in Figure 5d clearly shows an ordered phase. This phase crystallizes in the space group *Pnma* (Z = 4), exhibiting a coordination number of eight owing to the large size of the anion. The anion geometry is almost identical to those of other reported salts.[55]

The structures of [**3**]CF_3BF_3 in both phases are extensively disordered and not satisfactorily refined, similar to those of [**3**]SbF_6. The apparent crystal systems of phases I (90 K) and IV (248 K), based on the unit cell dimensions, are orthorhombic and tetragonal, respectively (Z = 2). The PXRD patterns of this salt, shown in Figure S7b, are similar to those of [**3**]SbF_6 (Figure S7a). In particular, the patterns of the high-temperature phases are almost identical to each other, indicating that their structures are isomorphic, which is reasonable considering their similar anion volumes.

Crystal Structure of FSA Salts. The FSA salts [**1**]FSA−[**3**]FSA have a lower crystal symmetry than the other salts, reflecting their low anion symmetry.

The structures of [**1**]FSA at 90 K (phase I) and 333 K (phase II) are shown in Figure 5e. Phase I crystallizes in space group $P2_1/c$ (Z = 4) and exhibits an ordered structure, whereas phase II crystallizes in space group $C2/c$ (Z = 4) and exhibits extensive disorder. The molecular long axes of the cations are canted with each other in phase I, but they are nearly parallel in phase II (Figure 5e). The cation in phase II is refined as twofold disordered by rotation (occupancy ratio 0.516(15):0.484(15)), and the anion is also refined as disordered with two equally occupied symmetry equivalent moieties. Such order−disorder in the FSA anion upon phase transition is often observed.[56−59] The coordination number change from six in phase I to eight in phase II is ascribed to an effective change in the radius ratio caused by the disorder of the anion. These large structural changes are consistent with the large transition entropy (30.6 J mol K^{-1}).

The crystal structures of [**2**]FSA and [**3**]FSA at 90 K (phase I) are shown in Figure 5f−g. They crystallize in the space groups $P2_1/c$ and $P2_1/n$, respectively (Z = 4). The cations in both structures are ordered, but the anion in [**2**]FSA exhibits twofold disorder (occupancy ratio 0.581(5):0.419(5)). The proximity of their melting points prevented the collection of diffraction data for phase II in these salts.

Ligand Exchange Reactions. To explore the solid-state reactivity of Rh−cod complexes, we investigated the ligand exchange reactions of SbF_6 salts using single crystals and found that [**3**]SbF_6 and [**2**]SbF_6 undergo an in situ SC−SC reaction.

Single crystals of [**3**]SbF_6 (0.5 mg, typical size: ∼150 × 50 × 50 μm^3) were immersed in diethyl ether (5 mL), followed by the addition of a very small amount of the coordinating solvent (SMe_2 or CH_3CN, 4 μL). The sample was left to stand for 3 days, during which the ligand exchange reaction proceeded gradually in an SC−SC manner (Figure 7a,b and Table 2). [**3**]SbF_6 and its products were yellow crystals insoluble in the solvent, and the structures of the SC−SC reaction products [**4**]SbF_6 and [**5**]SbF_6 were confirmed by single-crystal X-ray structural analysis (see below). The reaction occurred on the surface, which was visually observable under a polarizing optical microscope, as thick crystals did not allow the reaction to proceed into the interior. This resulted in overall conversions of 52 and 14%, respectively, over 3 days, as confirmed by ^{1}H NMR spectra.

Single crystals of [**2**]SbF_6 (∼50 × 50 × 20 μm^3) also exhibited SC−SC ligand exchange reactions for SMe_2 and CH_3CN under similar conditions, with overall conversions of 92 and 17%, respectively (Table 2). The higher conversion compared to that of [**3**]SbF_6 is ascribed to its smaller crystal size.

Interestingly, the addition of a large excess of SMe_2 to dissolve [**3**]SbF_6 in air resulted in the deposition of a mixture of [**4**]SbF_6 and of the new salt [$Rh(C_8H_{12}O)(SMe_2)_3$]SbF_6 ([**6**]SbF_6) over the range of 2 weeks. The cation of the latter consists of a ligand and central metal in the oxidized state. The structure determined by crystallographic analysis is shown in Figure 7c. The formation of similar compounds by the oxidation of cod complexes is known;[60,61] hence, the reaction observed here probably also occurred by the air oxidation of the cation in solution.

In contrast, the reaction of [**1**]SbF_6 proceeded in a considerably shorter time without maintaining crystallinity.

https://doi.org/10.1021/acs.inorgchem.2c03865
Inorg. Chem. 2023, 62, 2169−2180

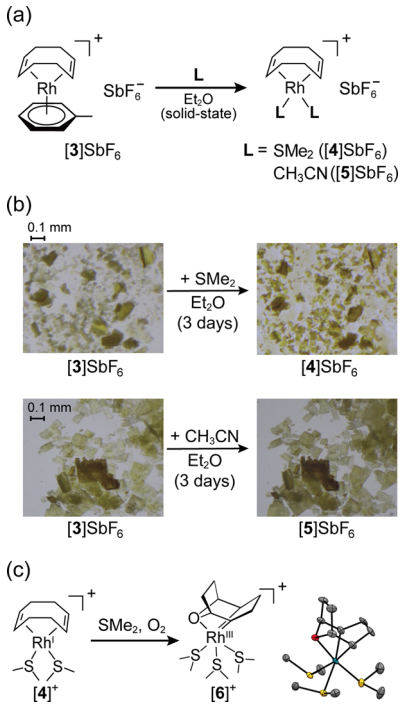

Figure 7. (a) In situ ligand exchange reaction of single crystals of $[3]SbF_6$ performed in a diethyl ether medium. (b) Conversion from $[3]SbF_6$ to $[4]SbF_6$ or $[5]SbF_6$, captured for the same samples during ligand exchange reactions in ether. (c) Oxidation reaction of $[4]^+$. The X-ray structure of the cation is shown on the right.

The reaction of $[1]SbF_6$ with SMe_2 and CH_3CN in diethyl ether proceeded in 76% (in a day) and 100% (in 1 h) yields, respectively, both changing from red-brown crystals to lumpy yellow amorphous solids (Table 2, Figure S9). The reaction with SMe_2 was slower than that with CH_3CN. The faster reaction of $[1]SbF_6$ than those of $[2]SbF_6$ and $[3]SbF_6$ is probably ascribed to the easier dissociation of the cod ligand than that of the arene ligands,[34] which is also consistent with their thermal decomposition behavior (Figure 4a).

For comparison, the direct reactions of single crystals of $[1]SbF_6$ and $[3]SbF_6$ with solvent vapors were examined. The reactions proceeded quantitatively in a considerably shorter time without maintaining crystallinity (Figure S10). Exposure to SMe_2 vapor for 5 min produced amorphous products, even for $[3]SbF_6$, indicating that a very fast reaction results in crystallinity loss. Exposure to CH_3CN vapor resulted in the formation of yellow liquids, which is ascribed to the presence of released ligands in the products. Therefore, the use of ether as a medium is advantageous to slow down the reaction speed because of dilution, and the released ligand is efficiently removed, preventing the formation of an oily mixture.

$[2]SbF_6$ and $[3]SbF_6$ are both dynamically disordered crystals, and this feature may facilitate the SC-SC reactions. However, because both salts undergo the SC−SC reaction in a similar manner, the correlation between reactivity and rotational phase is not clear from the current experiments. Although many examples of SC−SC reactions in coordination compounds have already been reported,[62] the current reaction is important because it involves Rh−cod precatalysts and can be potentially extended to solid-state catalytic reactions. In the current SC−SC reactions, ether may have a role in assisting molecular diffusion at the surface, similar to solvent-assisted solid-state reactions.[63] These points require further investigation.

Characterization of the Ligand-Exchanged Products. The crystal structures of the single crystals of $[4]SbF_6$ and $[5]SbF_6$ obtained via in situ SC−SC ligand exchange were determined along with their thermal properties.

The structure of the as-formed crystal of $[4]SbF_6$ determined at 90 K (phase I) is shown in Figure 8a. This salt crystallizes in the triclinic space group $P\text{-}1$ ($Z = 2$) with a coordination number of six. One cation and two half anions are crystallographically independent, and the Rh−S bond distances are 2.370(1) and 2.3824(9) Å, respectively. The crystal structures of $[5]SbF_6$ were determined at 90 K (phase I) and 293 K (phase II) because of the phase transition at 136 K (see below). We also confirmed that the crystal structure of $[5]SbF_6$ synthesized by the SC−SC reaction is identical to that obtained by recrystallization of an authentic sample from dichloromethane-diethyl ether (Table S3). Phase I crystallizes in space group $C2/c$ ($Z = 8$). Two half pairs of cations and anions are present in the asymmetric unit of the structure and are crystallographically independent, and all four ions are located on the crystallographic twofold axes. Phase II crystallizes in space group $Fddd$ ($Z = 16$). The crystal symmetry is higher, and the unit cell volume is twice that of phase I, but the molecular arrangements are almost identical (Figures 8b and S11). One half cation, located on a twofold axis, and two quarters of the occupied anions, located at the intersections of two twofold axes, are crystallographically independent. Anion I is surrounded by acetonitrile molecules and is ordered, whereas anion II is surrounded by cod and is refined as twofold disordered by rotation (occupancy ratio 0.876(8):0.124(8)), probably because of the larger space surrounding the anion. The small transition entropy from phase I to II (4.4 J mol K^{-1}) is consistent with this rather small structural change. The cation has Rh−N bond lengths of 2.07−2.08 Å and exhibits virtually identical structure as that in $[5]BF_4$.[6]

DSC measurements revealed no phase transitions for $[4]SbF_6$ and decomposition at 433 K without melting, whereas $[5]SbF_6$ exhibited a solid phase transition at 136.0 K ($\Delta S = 4.4$ J mol^{-1} K^{-1}), followed by melting at 410.6 K ($\Delta S_m = 61.7$ J mol^{-1} K^{-1}, Figure S1a). Its melting point is approximately 50 K lower than that of $[5]BF_4$ (T_m = 461−463 K[64]). Upon cooling from the melt, the salt exhibited glass transition at

Table 2. Morphology of Products Formed by In Situ Reactions of $[1]SbF_6$−$[3]SbF_6$ with Coordinating Molecules (L′) Using Single Crystals [SC = Single Crystal, A = Amorphous][a]

	reaction in diethyl ether			reaction with vapor (5 min)	
L′	$[1]SbF_6$	$[2]SbF_6$	$[3]SbF_6$	$[1]SbF_6$	$[3]SbF_6$
SMe_2	A (76%, 1 day)	SC (92%, 3 days)	SC (52%, 3 days)	A (99%)	A (98%)
MeCN	A (100%, 1 h)	SC (17%, 3 days)	SC (14%, 3 days)	oil[b]	oil[b]

[a]Conversion and reaction time are shown in parenthesis. [b]Oil is gradually formed during reaction.

https://doi.org/10.1021/acs.inorgchem.2c03865
Inorg. Chem. 2023, 62, 2169−2180

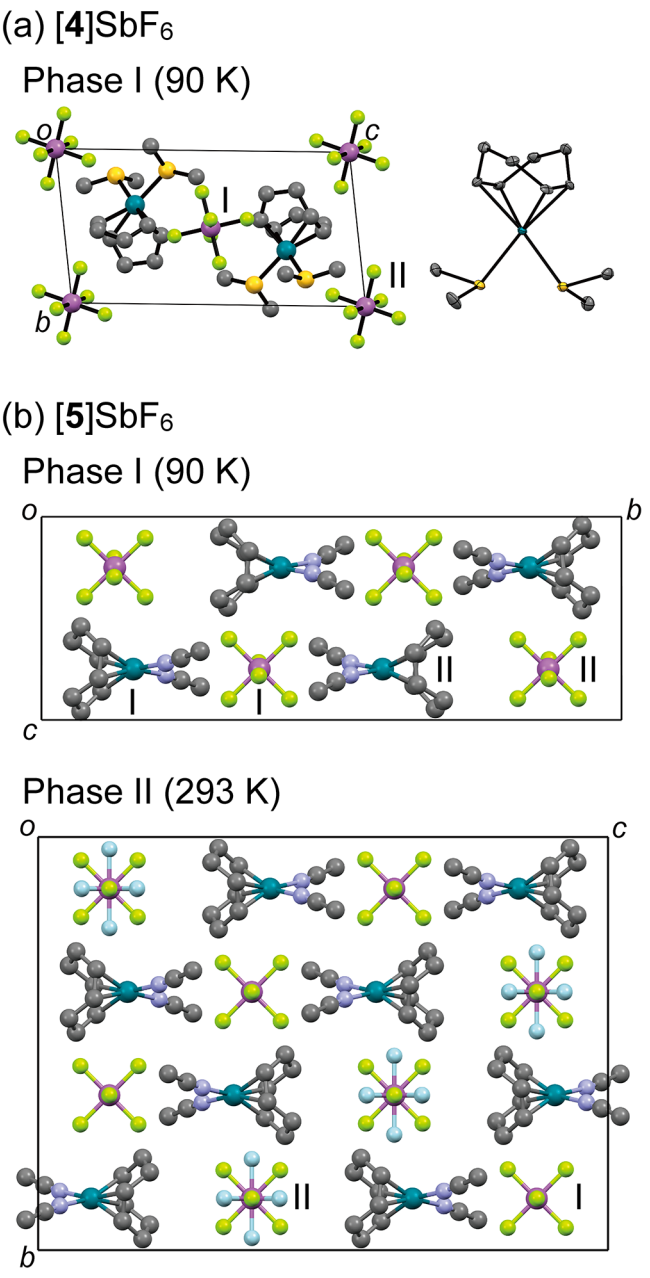

Figure 8. Packing diagrams of (a) [**4**]SbF_6 and (b) [**5**]SbF_6. ORTEP drawing of the cation is shown in (a). Crystallographically independent molecules are labeled as I and II.

279.8 K, and cold crystallization and melting occurred during its reheating.

The TG charts for these salts are shown in Figure 9. The decomposition temperature (3 wt %) of [**4**]SbF_6 is 433 K, and a slight weight loss starts at approximately 350 K. The loss of the two SMe_2 molecules occurs in two steps, exhibiting a weight loss of approximately 10 wt % in each step, up to 460 and 520 K (calculated value for the loss of one SMe_2: 11 wt %), and a weight loss of approximately 34 wt % is observed between 520 and 600 K, which corresponds to the losses of cod and some SbF_5 formed by partial decomposition of the anion. The decomposition temperature (−3 wt %) of [**5**]SbF_6 is 441 K, exhibiting a one-step weight loss of 36 wt % up to 518 K. This corresponds to the loss of two acetonitrile molecules and cod (calculated value: 36 wt %). These salts are less

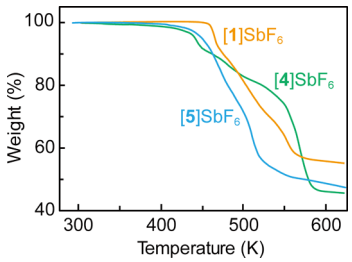

Figure 9. TG curves of [**1**]SbF_6, [**4**]SbF_6, and [**5**]SbF_6, measured at a scan rate of 3 K min^{-1} in a nitrogen atmosphere.

thermally stable than [**1**]SbF_6 and exhibit ligand desorption at lower temperatures. In particular, the slight weight loss initiated at relatively low temperatures in [**4**]SbF_6 is consistent with its tendency to gradually decompose in air. Furthermore, the slower reaction of [**1**]SbF_6 with SMe_2 than with CH_3CN in diethyl ether (Table 2) is consistent with the lower thermal stability of [**4**]SbF_6 than that of [**5**]SbF_6.

The syntheses of structurally related salts, [**5**]ClO_4,[65] $[Rh(cod)(dmso)_2]BF_4$,[66] and $[Rh(cod)(H_2O)_2]OTf$,[67] have been reported, of which $[Rh(cod)(dmso)_2]BF_4$ and $[Rh(cod)(H_2O)_2]OTf$ have been structurally characterized. $[Rh(cod)(H_2O)_2]OTf$ exhibits a phase transition at 215 K,[67] where the order−disorder of the anion occurs, similar to [**4**]SbF_6.

CONCLUSIONS

In this study, the thermal properties and crystal structures of cationic Rh−cod complexes with cyclic ligands were investigated. These salts exhibit solid phase transitions, through which the disorder and crystal symmetry increase in higher-temperature phases. Crystal symmetry typically depends on the anion, whereas less symmetrical cations tend to exhibit more severely disordered phases. [Rh(cod)(PhMe)]SbF_6 exhibits a rotator phase at room temperature, whereas the other salts exhibit dynamically disordered phases. In contrast to the salts of sandwich complexes, no structurally isotropic IPC phase was found owing to the elongated, ellipsoidal shape of the cations. We also investigated the thermal stabilities and chemical reactivities of these salts. FSA salts with arene ligands undergo ligand exchange reactions upon melting, leading to lower thermal stability. Salts with arene ligands undergo in situ ligand exchange in ether via an SC−SC reaction. The insights obtained in this study provide fundamental information that is useful for the development and application of organometallic reactions because the catalytic reactivities of Rh−cod complexes are based on their coordination abilities. Furthermore, this knowledge will be useful for the future exploration of organometallic solid-state reaction chemistry, including catalytic reactions.

EXPERIMENTAL SECTION

General. All reactions were performed under a nitrogen atmosphere, and dehydrated solvents were used. $[M(cod)_2]SbF_6$ (M = Rh, Ir),[35] $[Rh(cod)_2]BF_4$,[68] AgFSA,[40] and $AgCB_{11}H_{12}$[69] were synthesized according to previously reported procedures. $AgCF_3BF_3 \cdot nCH_3CN$ was obtained as a hygroscopic white powder by the reaction of KCF_3BF_3 and silver nitrate in acetonitrile. The white precipitate of potassium nitrate formed during the reaction was removed by filtration, and the filtrate was concentrated, followed by the addition of diethyl ether. The desired compound precipitated after standing the solution at 233 K for a day, which was collected by filtration. Other reagents were purchased from TCI. ^1H NMR spectra were

https://doi.org/10.1021/acs.inorgchem.2c03865
Inorg. Chem. 2023, 62, 2169−2180

recorded on a Bruker Advance 400 spectrometer. FTIR spectra were acquired using a Thermo Nicolet iS5 spectrometer fitted with attenuated total reflectance (ATR). DSC measurements were performed using a TA Q100 differential scanning calorimeter at a scan rate of 10 K min^{-1} using aluminum hermetic pans as sample containers. TG-DTA measurements were performed using a Rigaku TG8120 thermal analyzer at a scan rate of 3 K min^{-1} under a nitrogen atmosphere. Solid-state NMR spectra were recorded on a Tecmag Apollo spectrometer (operating at 46.045 MHz for ^2H and 299.95 2 MHz for ^1H) equipped with a Doty XC MAS 4 mm probe head. The ^1H NMR spectra were measured with a 3.9 μs $\pi/2$ pulse. The ^2H spectra were measured with a solid echo pulse sequence [$\pi/2 - \tau - \pi/2 - \tau -$ acquisition],[70] using a 4.6 μs $\pi/2$ pulse and a delay time τ of 40 μs. The recycle delays for the ^1H and ^2H measurements were 7 s and 3 s, respectively.

Synthesis of Metal Complexes. *[Rh(cod)$_2$]X ([1]X; X = FSA, $CB_{11}H_{12}$, CF_3BF_3).* These salts were synthesized using a method similar to that of [Rh(cod)$_2$]SbF_6.[35] The synthesis of [Rh(cod)$_2$]FSA is described below as an example. 1,5-Cyclooctadiene (29 mg, 0.31 mmol) was added to a solution of [Rh(cod)Cl]$_2$ (50 mg, 0.10 mmol) in dichloromethane (2 mL) under stirring. An acetone solution (1 mL) of AgFSA (79 mg, 0.23 mmol) was added, and a white precipitate was immediately formed. The suspension was stirred for 1 h, and the white solid was removed by Celite filtration. The filtrate was concentrated using a rotary evaporator, to which hexane (5 mL) was added. A reddish-brown oil phase containing the desired product was separated, the hexane phase was removed with a pipette, and the remaining oil was washed with hexane (5 mL × 2) and diethyl ether (5 mL × 3). The remaining solvent was removed under reduced pressure, and recrystallization of the resultant solid from dichloromethane-diethyl ether at 233 K resulted in the desired product as reddish brown crystals (78 mg, 78% yield). ^1H NMR (400 MHz, $CDCl_3$): δ = 2.47−2.68 (m, 16H, CH_2), 5.34 (br, 8H, CH). FTIR (ATR, cm^{-1}): 564, 736, 823, 1105, 1171, 1360, 1427, 2891. Anal. calcd. for $C_{16}H_{24}F_2NO_4RhS_2$: C, 38.48; H, 4.84; N, 2.80. Found: C, 38.42; H, 5.02; N, 2.87. The other salts were synthesized in a similar manner using the corresponding silver salts. [Rh(cod)$_2$]$CB_{11}H_{12}$: reddish brown crystals (20% yield). ^1H NMR (400 MHz, $CDCl_3$): δ = 0.81−0.91 (br, 11H, BH), 2.18 (s, 1H, $CHBH_{11}$) 2.35−2.54 (m, 16H, CH_2), 5.11 (br, 1H, cod−CH), 5.29 (br, 2H, cod−CH), 5.59 (br, 5H, cod−CH). FTIR (ATR, cm^{-1}): 716, 783, 860, 1001, 1023, 1065, 1426, 1472, 2509. Anal. calcd. for $C_{17}H_{36}B_{11}Rh$: C, 44.17; H, 7.85; N, 0.00. Found: C, 43.55; H, 7.40; N, 0.12. [Rh(cod)$_2$]CF_3BF_3: reddish brown crystals (29% yield). ^1H NMR (400 MHz, $CDCl_3$): δ = 2.46−2.69 (m, 8H, CH_2), 5.33 (br, 4H, CH). FTIR (ATR, cm^{-1}): 632, 783, 829, 862, 946, 970, 1043, 1430. Anal. calcd. for $C_{17}H_{24}BF_6Rh$: C, 44.77; H, 5.30; N, 0.00. Found: C, 44.67; H, 5.36; N, 0.07.

[Rh(cod)L]X ([2]X: L = C_6H_6, [3]X: L = PhMe, X = SbF_6, FSA). The synthesis of [Rh(cod)(PhMe)]SbF_6 is described below as an example. Toluene (325 mg, 3.5 mmol) was added to a solution of [Rh(cod)Cl]$_2$ (349 mg, 0.81 mmol) in dichloromethane (5 mL) with stirring. In sequence, a solution of $AgSbF_6$ (510 mg, 1.7 mmol) in acetone (1 mL) was added to this solution to form a white precipitate. The suspension was stirred for 1 h, and the solid was removed by Celite filtration. The filtrate was concentrated using a rotary evaporator, followed by addition of hexane (5 mL). A yellow oil phase containing the desired product was separated, the hexane phase was removed using a pipette, and the remaining oil was washed with hexane (5 mL × 2) and diethyl ether (5 mL × 3). The remaining solvent was removed under reduced pressure, and recrystallization of the resultant solid from dichloromethane-diethyl ether (233 K) resulted in the desired product as yellow crystals (618 mg, yield 81%). ^1H NMR (400 MHz, $CDCl_3$): δ = 2.08−2.17 (m, 8H, CH_2), 2.35−2.45 (m, 8H, CH_2), 2.39 (s, 3H, CH_3), 4.65 (br, 4H, CH), 6.68−6.74 (m, 3H, arene−H), 6.77−6.82 (m, 2H, arene−H). FTIR (ATR, cm^{-1}): 647, 807, 889, 990, 1165, 1452, 1549. Anal. calcd. for $C_{15}H_{20}F_6RhSb$: C, 33.43; H, 3.74; N, 0.00. Found: C, 33.37; H, 3.77; N, 0.08. The corresponding deuterated complex [Rh(cod)-($C_6D_5CD_3$)]SbF_6 (*d*-[**3**]SbF_6) was synthesized using toluene-d_8 (84% yield). The other salts were synthesized in a similar manner using the corresponding ligands and silver salts. [Rh(cod)(C_6H_6)]-SbF_6: Yellow crystals (19% yield). ^1H NMR (400 MHz, $CDCl_3$): δ = 2.11−2.19 (m, 4H, CH_2), 2.36−2.46 (m, 4H, CH_2), 4.83 (br, 4H, *CH*), 6.87 (s, 6H, C_6H_6). FTIR (ATR, cm^{-1}): 647, 785, 827, 891, 990, 1010, 1163, 1309, 1337, 1443, 1464. Anal. calcd. for $C_{14}H_{18}F_6RhSb$: C, 32.03; H, 3.46; N, 0.00. Found: C, 31.81; H, 3.38; N, 0.08. The corresponding deuterated complex [Rh(cod)-(C_6D_6)]SbF_6 (*d*-[**1**]SbF_6) was synthesized using benzene-d_6 and acetone as the solvents. In this case, benzene-d_6 was added to the recrystallization solvent to suppress ligand dissociation (60% yield). [Rh(cod)(PhMe)]FSA: Yellow crystals (45% yield). ^1H NMR (400 MHz, $CDCl_3$): δ = 2.11−2.20 (m, 4H, CH_2), 2.35−2.45 (m, 4H, CH_2), 2.42 (s, 3H, CH_3), 4.67 (br, 4H, CH), 6.72−6.78 (m, 3H, arene−H), 6.81−6.87 (m, 2H, arene−H). FTIR (ATR, cm^{-1}): 564, 727, 826, 1101, 1174, 1216, 1360, 1451, 2842. Anal. calcd. for $C_{15}H_{20}F_2NO_4RhS_2$: C, 37.27; H, 4.17; N, 2.90. Found: C, 37.27; H, 4.19; N, 2.83. [Rh(cod)(C_6H_6)]FSA: Yellow crystals (19% yield). ^1H NMR (400 MHz, $CDCl_3$): δ = 2.11−2.19 (m, 4H, CH_2), 2.36−2.46 (m, 4H, CH_2), 4.83 (br, 4H, CH), 6.87 (s, 6H, C_6H_6). FTIR (ATR, cm^{-1}): 563, 737, 824, 1098, 1171, 1360, 1549, 1622, 2955. Anal. calcd. for $C_{14}H_{18}F_2NO_4RhS_2$: C, 35.83; H, 3.87; N, 2.98. Found: C, 35.34; H, 3.76; N, 2.91.

[Rh(cod)(PhMe)]CF_3BF_3 ([3]CF_3BF_3). The salt was prepared using a similar method to that of [Rh(cod)(PhMe)]BF_4.[34] Toluene (1 mL) was added to a solution of [Rh(cod)$_2$]CF_3BF_3 (26 mg, 0.05 mmol) in dichloromethane (2 mL) under stirring, and the mixture was further stirred for 3 days. The solution was concentrated using a rotary evaporator, followed by addition of diethyl ether (10 mL). Subsequently, a pale orange solid precipitated and was collected by filtration. Recrystallization from dichloromethane/diethyl ether (233 K) yielded orange crystals (21 mg, 84% yield). ^1H NMR (400 MHz, $CDCl_3$): δ = 2.08−2.17 (m, 4H, CH_2), 2.34−2.44 (m, 4H, CH_2), 2.39 (s, 3H, CH_3), 4.65 (br, 4H, CH), 6.70−6.77 (m, 3H, arene−H), 6.79−6.84 (m, 2H, arene−H). FTIR (ATR, cm^{-1}): 631, 782, 828, 863, 947, 970, 1043, 1429, 1449. Anal. calcd. for $C_{12}H_{18}F_6N_2RhSb$: C, 43.67; H, 4.58; N, 0.00. Found: C, 43.48; H, 4.74; N, 0.00.

[Rh(cod)(CH_3CN)$_2$]SbF_6 ([5]SbF_6). Diethyl ether (5 mL) was added to a solution of [Rh(cod)$_2$]SbF_6 (30 mg, 0.05 mmol) in acetonitrile (1 mL). A yellow solid was precipitated, which was collected by filtration, and recrystallization of the solid from dichloromethane-diethyl ether at 233 K yielded yellow crystals. The second crop was also collected and combined (76% yield). ^1H NMR (400 MHz, $CDCl_3$): δ = 1.86−1.96 (m, 4H, CH_2), 2.35 (s, 6H, CH_3), 2.44−2.54 (m, 4H, CH_2), 4.40 (br, 4H, CH). FTIR (ATR, cm^{-1}): 652, 877, 981, 1005, 1027, 1082, 1166, 1228, 1314, 1337, 1409, 1437, 2284, 2311. Anal. calcd. for $C_{12}H_{18}F_6N_2RhSb$: C, 27.75; H, 3.43; N, 5.30. Found: C, 27.40; H, 3.31; N, 5.16.

Ligand Exchange Reactions. Ligand exchange reactions using single crystals of [**2**]SbF_6 and [**3**]SbF_6 were performed in diethyl ether. The crystals (0.5 mg) were placed in diethyl ether (5 mL) under a nitrogen atmosphere. These salts were insoluble in ether. A small amount of SMe_2 or acetonitrile (4 μL) was added to the solvent, which was left unperturbed, and the solids were gradually converted to [Rh(cod)(SMe_2)$_2$]SbF_6 ([**4**]SbF_6) and [**5**]SbF_6 without any change in appearance. The conversions of [**2**]SbF_6 to [**4**]SbF_6 and [**5**]SbF_6 were 92 and 17%, respectively, whereas those of [**3**]SbF_6 were 52 and 14%, respectively, as determined using ^1H NMR spectroscopy ($CDCl_3$). The reactions of [**1**]SbF_6 with SMe_2 or acetonitrile were performed in a similar manner. In this case, the appearance changed from reddish-brown block crystals to yellow solids, and the conversions were 76% (1 day) and 100% (after 1 h) for the reactions with SMe_2 and acetonitrile, respectively. The crystals of [**4**]SbF_6 gradually decomposed in air and turned green over a few days. To avoid possible degradation, the samples recrystallized from dichloromethane-diethyl ether (233 K) were immediately used for the TG-DTA and DSC measurements. [**4**]SbF_6: ^1H NMR (400 MHz, $CDCl_3$): δ = 2.06−2.18 (m, 4H, CH_2), 2.31 (s, 12H, CH_3), 2.50−2.63 (m, 4H, CH_2), 4.55 (br, 4H, CH). FTIR (ATR, cm^{-1}): 649, 857, 980, 1031, 1306, 1335, 1430. Anal. calcd. for $C_{12}H_{18}F_6N_2RhSb$: C,

https://doi.org/10.1021/acs.inorgchem.2c03865
Inorg. Chem. 2023, 62, 2169−2180

25.24; H, 4.24; N, 0. Found: C, 24.84; H, 3.65; N, 1.17. The discrepancy in the analytical data was ascribed to slight decomposition. Upon addition of a large excess of SMe_2 (0.5 mL) to [**3**]SbF_6 (0.5 mg) in diethyl ether, part of the crystal dissolved, and upon standing the solution, a solid mixture of [**4**]SbF_6 and an oxidation product $[Rh(C_8H_{12}O)(SMe_2)_3]SbF_6$ ([**6**]SbF_6) (molar ratio ~ 0.8:0.2) were deposited over 2 weeks. The structure of the latter was determined using X-ray crystallography. [**6**]SbF_6:^{1}H NMR (400 MHz, $CDCl_3$): δ = 2.08 (m, 4H, $RhCHCH_2$-*endo*, $OCHCH_2$-*endo*), 2.59 (m, 4H, $RhCHCH_2$-*exo*, $OCHCH_2$-*exo*), 2.63 (s, 9H, CH_3), 3.04 (m, 2H, RhCH), 5.87 (m, 2H, OCH).

The reactions with solvent vapors were performed as follows: A small vial (1 mL) containing [**1**]SbF_6 or [**3**]SbF_6 crystals (0.5 mg) was placed in a larger vial (10 mL) under a nitrogen atmosphere. A small amount of the solvent (CH_3CN or SMe_2; 0.1 mL) was placed in an outer vial, sealed, and allowed to stand at room temperature for 5 min. [**1**]SbF_6 and [**3**]SbF_6 reacted with SMe_2 vapor to form [**4**]SbF_6 as a yellow amorphous solid in almost quantitative yield. The conversion was confirmed using ^{1}H NMR spectroscopy ($CDCl_3$). The reactions with CH_3CN vapor proceeded quantitatively to result in a yellow liquid, which yielded solid [**5**]SbF_6 after vacuum-drying.

X-Ray Crystallography. X-ray diffraction data were collected using a Bruker APEX II Ultra diffractometer (X-ray source: Mo*K*α rotating anode), and calculations were performed using SHELXL[71] (software: APEX3[72]). Packing diagrams were drawn using Mercury software,[73] and the packing indices were calculated using Platon.[74] [**1**]CF_3BF_3 (phase II) and [**5**]SbF_6 (phase I) were twinned; therefore, TWINABS[75] was used for scaling and empirical absorption correction, and the second component contribution was modeled using the HKLF5 refinement. PXRD patterns were calculated using XPREP[76] from the single-crystal *hkl* reflection data. The unit cell parameters were based on single-crystal unit cell determination. The crystallographic parameters are listed in Tables S1−S7. For the structural determination of [**3**][Rh(cod)$(FSA)_2$], single crystals formed from a molten liquid of [**3**]FSA were used, and the data were collected at 388 K to prevent solidification of unreacted [**3**]FSA. The data quality was less satisfactory because of the high data collection temperature and gradual crystal degradation. Other crystals were obtained by recrystallization from organic solvents. CSD numbers: CCDC-2183669−2183683 and 2193891 contain the crystallographic data for [**1**]SbF_6, [**1′**]SbF_6, [**2**]SbF_6, [**2**]SbF_6 (phase II), [**1**]FSA, [**1**]FSA (phase II), [**2**]FSA, [**3**]FSA, [**1**]CF_3BF_3, [**1**]CF_3BF_3 (phase II), [**1**]$CB_{11}H_{12}$, [**5**]SbF_6, [**5**]SbF_6 (phase II), [**4**]SbF_6, [**3**][Rh(cod)$(FSA)_2$], and [**6**]SbF_6.

■ ASSOCIATED CONTENT

Supporting Information

The Supporting Information is available free of charge at https://pubs.acs.org/doi/10.1021/acs.inorgchem.2c03865.

DSC charts, POM images, crystal structures, TG-DTA charts, PXRD patterns, infrared spectra, and crystallographic parameters (PDF)

Accession Codes

CCDC 2183669−2183683 and 2193891 contain the supplementary crystallographic data for this paper. These data can be obtained free of charge via www.ccdc.cam.ac.uk/data_request/cif, or by emailing data_request@ccdc.cam.ac.uk, or by contacting The Cambridge Crystallographic Data Centre, 12 Union Road, Cambridge CB2 1EZ, UK; fax: +44 1223 336033.

■ AUTHOR INFORMATION

Corresponding Author

Tomoyuki Mochida − *Department of Chemistry, Graduate School of Science and Research Center for Membrane and Film Technology, Kobe University, Kobe, Hyogo 657-8501, Japan*; orcid.org/0000-0002-3446-2145; Phone: +81-78-803-5679; Email: tmochida@platinum.kobe-u.ac.jp

Authors

Ryo Sumitani − *Department of Chemistry, Graduate School of Science, Kobe University, Kobe, Hyogo 657-8501, Japan*

Daisuke Kuwahara − *Graduate School of Informatics and Engineering, The University of Electro-Communications, Chofu, Tokyo 182-8585, Japan*

Complete contact information is available at: https://pubs.acs.org/10.1021/acs.inorgchem.2c03865

Notes

The authors declare no competing financial interest.

■ ACKNOWLEDGMENTS

This work was financially supported by KAKENHI (grant number: 20H02756) from the Japan Society for the Promotion of Science (JSPS) and a Grant-in-Aid for JSPS Research Fellows (grant number: 21J12056). We are grateful to the anonymous reviewers for their valuable comments.

■ REFERENCES

(1) Ojima, I.; Vu, A. T.; Bonafoux, D. Product Class 5: Organometallic Complexes of Rhodium. In *Science of Synthesis*; Lautens, M., Ed.; Thieme Verlag, 2001; pp 531−616.

(2) Garralda, M. A.; Oro, L. A. Cationic Rhodium(I) Diolefin Complexes. *Transition Met. Chem.* **1980**, *5*, 65−73.

(3) Osborn, J. A.; Schrock, R. R. Coordinatively Unsaturated Cationic Complexes of Rhodium(I), Iridium(I), Palladium(II), and Platinum(II). Generation, Synthetic Utility, and Some Catalytic Studies. *J. Am. Chem. Soc.* **1971**, *93*, 3089−3091.

(4) Emerson-King, J.; Knighton, R. C.; Gyton, M. R.; Chaplin, A. B. Rotaxane Synthesis Exploiting the M(I)/M(III) Redox Couple. *Dalton Trans.* **2017**, *46*, 11645−11655.

(5) Wender, P. A.; Williams, T. J. [(arene)Rh(cod)]$^+$ Complexes as Catalysts for [5+2] Cycloaddition Reactions. *Angew. Chem., Int. Ed.* **2002**, *41*, 4550−4553.

(6) Kang, S. O.; Lynch, V. M.; Day, V. W.; Anslyn, E. V. Enthalpy- vs Entropy-Driven Complexation of Homoallylic Alcohols by Rhodium-(I) Complexes. *Organometallics* **2011**, *30*, 6233−6240.

(7) Toda, F., Ed.; *Organic Solid State Reactions*; Springer: Berlin Heidelberg, 2005.

(8) Sheng, M.; Yang, Q.; Huff, D.; Schafer, A. G.; Tucker, C.; Valco, D. Thermal Instability and Associated Potential Safety Hazards of Rhodium(I) Precatalyst Complexes with Weakly Coordinated Ligands. *Org. Process Res. Dev.* **2021**, *25*, 1054−1064.

(9) Togni, A.; Hayashi, T., Eds.; *Ferrocenes: Homogeneous Catalysis, Organic Synthesis, Materials Science*; Wiley-VCH Verlag: Weinheim, Germany, 1995.

(10) Stepnicka, P., Ed.; *Ferrocenes: Ligands, Materials and Biomolecules*; Wiley-Blackwell: Hoboken, NJ, 2008.

(11) Webb, R. J.; Lowery, M. D.; Shiomi, Y.; Sorai, M.; Wittebort, R. J.; Hendrickson, D. N. Ferrocenium Hexafluorophosphate: Molecular Dynamics in the Solid State. *Inorg. Chem.* **1992**, *31*, 5211−5219.

(12) Grepioni, F.; Cojazzi, G.; Draper, S. M.; Scully, N.; Braga, D. Crystal Forms of Hexafluorophosphate Organometallic Salts and the Importance of Charge-Assisted C−H—F Hydrogen Bonds. *Organometallics* **1998**, *17*, 296−307.

(13) Mochida, T.; Funasako, Y.; Ishida, M.; Saruta, S.; Kosone, T.; Kitazawa, T. Crystal Structures and Phase Sequences of Metallocenium Salts with Fluorinated Anions: Effects of Molecular Size and Symmetry on Phase Transitions to Ionic Plastic Crystals. *Chem. −Eur. J.* **2016**, *22*, 15725−15732.

(14) Tominaga, T.; Ueda, T.; Mochida, T. Effect of Substituents and Anions on the Phase Behavior of Ru(II) Sandwich Complexes:

Exploring the Boundaries between Ionic Liquids and Ionic Plastic Crystals. *Phys. Chem. Chem. Phys.* **2017**, *19*, 4352−4359.
(15) Mochida, T.; Ishida, M.; Tominaga, T.; Takahashi, K.; Sakurai, T.; Ohta, H. Paramagnetic Ionic Plastic Crystals Containing the Octamethylferrocenium Cation: Counteranion Dependence of Phase Transitions and Crystal Structures. *Phys. Chem. Chem. Phys.* **2018**, *20*, 3019−3028.
(16) Kimata, H.; Mochida, T. Effects of Molecular Structure on Phase Transitions of Ionic Plastic Crystals Containing Cationic Sandwich Complexes. *Cryst. Growth Des.* **2018**, *18*, 7562−7569.
(17) Pringle, J. M. Recent Progress in the Development and Use of Organic Ionic Plastic Crystal Electrolytes. *Phys. Chem. Chem. Phys.* **2013**, *15*, 1339−1351.
(18) Ishida, H.; Iwachido, T.; Hayama, N.; Ikeda, R.; Terashima, M.; Nakamura, D. Self-Diffusion and Reorientation of Methylammonium Ions in $(CH_3NH_3)_2ZnCl_4$ Crystals as Studied by ^{1}H-NMR. *Z. Naturforsch., A* **1989**, *44*, 741−746.
(19) Matsumoto, K.; Harinaga, U.; Tanaka, R.; Koyama, A.; Hagiwara, R.; Tsunashima, K. The Structural Classification of the Highly Disordered Crystal Phases of $[N_n][BF_4]$, $[N_n][PF_6]$, $[P_n][BF_4]$, and $[P_n][PF_6]$ Salts (N_n^+ = Tetraalkylammonium and P_n^+ = Tetraalkylphosphonium). *Phys. Chem. Chem. Phys.* **2014**, *16*, 23616−23626.
(20) Enomoto, T.; Kanematsu, S.; Tsunashima, K.; Matsumoto, K.; Hagiwara, R. Physicochemical Properties and Plastic Crystal Structures of Phosphonium Fluorohydrogenate Salts. *Phys. Chem. Chem. Phys.* **2011**, *13*, 12536−12544.
(21) Zhou, Z.-B.; Matsumoto, H. Lithium-Doped, Organic Ionic Plastic Crystal Electrolytes Exhibiting High Ambient-Temperature Conductivities. *Electrochem. Commun.* **2007**, *9*, 1017−1022.
(22) Hayasaki, T.; Hirakawa, S.; Honda, H. New Ionic Plastic Crystals of NR_4BEt_3Me (R = Me and Et) and $NR_xR'_{4-x}BEt_3Me$ (R = Et, R′ = Me and Pr, x = 1−3) in a New Class of Plastic Crystals. *Bull. Chem. Soc. Jpn.* **2013**, *86*, 993−1001.
(23) Yunis, R.; Newbegin, T. W.; Hollenkamp, A. F.; Pringle, J. M. Ionic Liquids and Plastic Crystals with a Symmetrical Pyrrolidinium Cation. *Mater. Chem. Front.* **2018**, *2*, 1207−1214.
(24) MacFarlane, D. R.; Huang, J.; Forsyth, M. Lithium-Doped Plastic Crystal Electrolytes Exhibiting Fast Ion Conduction for Secondary Batteries. *Nature* **1999**, *402*, 792−794.
(25) Henderson, W. A.; Herstedt, M.; Young, V. G.; Passerini, S.; De Long, H. C.; Trulove, P. C. New Disordering Mode for $TFSI^-$ Anions: The Nonequilibrium, Plastic Crystalline Structure of Et_4NTFSI. *Inorg. Chem.* **2006**, *45*, 1412−1414.
(26) Harada, J. Plastic/Ferroelectric Molecular Crystals: Ferroelectric Performance in Bulk Polycrystalline Forms. *APL Mater.* **2021**, *9*, No. 020901.
(27) Basile, A.; Hilder, M.; Makhlooghiazad, F.; Pozo-Gonzalo, C.; MacFarlane, D. R.; Howlett, P. C.; Forsyth, M. Ionic Liquids and Organic Ionic Plastic Crystals: Advanced Electrolytes for Safer High Performance Sodium Energy Storage Technologies. *Adv. Energy Mater.* **2018**, *8*, No. 1703491.
(28) Zhu, H.; MacFarlane, D. R.; Pringle, J. M.; Forsyth, M. Organic Ionic Plastic Crystals as Solid-State Electrolytes. *Trends Chem.* **2019**, *1*, 126−140.
(29) Yoshizawa-Fujita, M.; Nakazawa, M.; Takeoka, Y.; Rikukawa, M. Phase Transitions and Ionic Conductivity of Ionic Plastic Crystals Based on Pyrrolidinium Cations and Dihydrogen Phosphate Anion. *J. Non-Cryst. Solids: X* **2022**, *13*, No. 100078.
(30) Su, Y.; Liu, G.; Xie, B.; Fu, D.; Wang, D. Crystallization Features of Normal Alkanes in Confined Geometry. *Acc. Chem. Res.* **2014**, *47*, 192−201.
(31) Shimizu, T.; Tanaka, S.; Onoda-Yamamuro, N.; Ishimaru, S.; Ikeda, R. New Rotator Phase Revealed in Di-*n*-Alkylammonium Bromides Studied by Solid-State NMR, Powder XRD, Electrical Conductivity and Thermal Measurements. *J. Chem. Soc., Faraday Trans.* **1997**, *93*, 321−326.
(32) Pringle, J. M.; Shekibi, Y.; MacFarlane, D. R.; Forsyth, M. The Influence of Different Nanoparticles on a Range of Organic Ionic Plastic Crystals. *Electrochim. Acta* **2010**, *55*, 8847−8854.
(33) Yamada, Y.; Kashimoto, E.; Honda, H. New Chemical Family of $[n\text{-}C_xH_{(2x+1)}NEt_3][BEt_3Me]$ Showing Ionic Plastic-Crystal (x = 4, 5), Rotator-Crystal (x = 6, 7) and Liquid-Crystal Phases (x = 8−16). *Bull. Chem. Soc. Jpn.* **2019**, *92*, 1289−1298.
(34) Green, M.; Kuc, T. A. Cationic Transition-Metal Complexes. Part II. The Reaction of Arenes and Olefins with Bis(cyclo-octa-1,5-diene or Norbornadiene)Rhodium Tetrafluoroborate. *J. Chem. Soc., Dalton Trans.* **1972**, 832−839.
(35) RajanBabu, T. V.; Ayers, T. A.; Halliday, G. A.; You, K. K.; Calabrese, J. C. Carbohydrate Phosphinites as Practical Ligands in Asymmetric Catalysis: Electronic Effects and Dependence of Backbone Chirality in Rh-Catalyzed Asymmetric Hydrogenations Synthesis of *R*- or *S*-Amino Acids Using Natural Sugars as Ligand Precursors. *J. Org. Chem.* **1997**, *62*, 6012−6028.
(36) Song, G.; Zhang, Y.; Su, Y.; Deng, W.; Han, K.; Li, X. Pyridine-Based N-Heterocyclic Carbene Hydride Complexes of Iridium via C−H Activation. *Organometallics* **2008**, *27*, 6193−6201.
(37) Kar, M.; Matuszek, K.; MacFarlane, D. R. Ionic Liquids. In *Kirk-Othmer Encyclopedia of Chemical Technology*; John Wiley & Sons, Inc.: Hoboken, 2019.
(38) Sas, O. G.; Domínguez, I.; González, B.; Domínguez, Á. Liquid-Liquid Extraction of Phenolic Compounds from Water Using Ionic Liquids: Literature Review and New Experimental Data Using $[C_2mim]FSI$. *J. Environ. Manage.* **2018**, *228*, 475−482.
(39) Weller, A. S.; Mahon, M. F.; Steed, J. W. Rhodium Cyclooctadiene Complexes of the Weakly Co-Ordinating Carborane Anion $[Closo\text{-}CB_{11}H_{12}]^-$. Isolation and Crystal Structures of $[(COD)Rh(\eta^2\text{-}CB_{11}H_{12})]$ and $[(COD)Rh(THF)_2][CB_{11}H_{12}]$. *J. Organomet. Chem.* **2000**, *614*−*615*, 113−119.
(40) Tang, Y.; Yu, B. Coinage Metal (Bisfluorosulfonyl)Imide Complexes: Preparation, Characterization, and Catalytic Applications. *Eur. J. Inorg. Chem.* **2020**, *2020*, 107−118.
(41) Polyakov, O. G.; Ivanova, S. M.; Gaudinski, C. M.; Miller, S. M.; Anderson, O. P.; Strauss, S. H. $Cu(CO)_2(N(SO_2CF_3)_2)$. The First Structurally Characterized Copper(I) Polycarbonyl. *Organometallics* **1999**, *18*, 3769−3771.
(42) Begley, M. J.; Sowerby, D. B.; Verma, R. D.; Vig, A. Structure of the Silver Imidodi(sulphuryl fluoride)-Benzene Solvate $AgN(SO_2F)_2\cdot C_6H_6$. *J. Organomet. Chem.* **1994**, *481*, 243−246.
(43) Xiao, J.; Cui, Y.; Li, C.; Xu, H.; Zhai, Y.; Zhang, X.; Ma, S. Room Temperature Allenation of Terminal Alkynes with Aldehydes. *Angew. Chem., Int. Ed.* **2021**, *60*, 25708−25713.
(44) Bowring, M. A.; Bergman, R. G.; Tilley, T. D. Pt-Catalyzed C−C Activation Induced by C−H Activation. *J. Am. Chem. Soc.* **2013**, *135*, 13121−13128.
(45) Sievert, A. C.; Muetterties, E. L. Arene Transition-Metal Chemistry. 5. Arene Ligand Exchange and Reactivity in η^6-Arene Iridium(I) Complexes. *Inorg. Chem.* **1981**, *20*, 489−501.
(46) Guzel, B.; Omary, M. A.; Fackler, J. P.; Akgerman, A. Synthesis and Characterization of {[(COD)Rh(bis-(2R,3R)-2,5-diethylphospholanobenzene)]$^+$BARF$^-$} for Use in Homogeneous Catalysis in Supercritical Carbon Dioxide. *Inorg. Chim. Acta* **2001**, *325*, 45−50.
(47) Green, M.; Kuc, T. A.; Taylor, S. H. Cationic Transition-Metal Complexes. Part I. Synthesis and Reactions of Bis(diene)-Rhodium and -Iridium Tetrafluoroborates. *J. Chem. Soc. A* **1971**, 2334−2337.
(48) Mingos, D. M. P.; Rohl, A. L. Size and Shape Characteristics of Inorganic Molecules and Ions and Their Relevance to Molecular Packing Problems. *J. Chem. Soc., Dalton Trans.* **1991**, 3419−3425.
(49) Atkins, P.; Overton, T. *Shriver and Atkins' Inorganic Chemistry*; Oxford University Press: New York, 2010.
(50) Dahlenburg, L.; Osthoff, N.; Heinemann, F. W. Bis(η^4-Cyclo-octa-1,5-Diene)Rhodium(I) Trifluoromethanesulfonate. *Acta Crystallogr., Sect. E: Struct. Rep. Online* **2001**, *57*, 117−118.
(51) Baenziger, N. C.; Mottel, E. A.; Doyle, J. R. Structure of Bis(1,5-cyclooctadiene)rhodium(I) Hexacarbonyl-tri-μ-chloro-

https://doi.org/10.1021/acs.inorgchem.2c03865
Inorg. Chem. 2023, 62, 2169−2180

dirhenate(I). *Acta Crystallogr., Sect. C: Cryst. Struct. Commun.* **1991**, *47*, 539−541.
(52) Kotani, Y.; Honda, H. ^{1}H and ^{13}C NMR Studies on New Ionic Plastic Crystals Constructed by Ellipsoidal Cations with [BEt_3Me] Anion. *Bull. Chem. Soc. Jpn.* **2019**, *92*, 768−778.
(53) Rice, D. M.; Wittebort, R. J.; Griffin, R. G.; Meirovitch, E.; Stimson, E. R.; Meinwald, Y. C.; Freed, J. H.; Scheraga, H. A. Rotational Jumps of the Tyrosine Side Chain in Crystalline Enkephalin. ^{2}H NMR Line Shapes for Aromatic Ring Motions in Solids. *J. Am. Chem. Soc.* **1981**, *103*, 7707−7710.
(54) Emsley, J. W.; Lindon, J. C.; Tabony, J. Measurement of Deuterium Quadrupole Coupling Constants of CD_3 Groups by ^{1}H−{^{2}H} N.M.R. Studies of Nematic Solutions. *Mol. Phys.* **1973**, *26*, 1499−1509.
(55) Kimata, H.; Sumitani, R.; Mochida, T. Phase Transitions and Crystal Structures of Ionic Plastic Crystals Comprising Quaternary Ammonium Cations and Carborane Anion. *Chem. Lett.* **2019**, *48*, 859−862.
(56) Sumitani, R.; Funasako, Y.; Mochida, T. Thermal Properties and Crystal Structures of Ruthenium-Containing Photoreactive Ionic Liquids with Short Substituents. *J. Mol. Liq.* **2020**, *318*, No. 114071.
(57) Matsumoto, K.; Oka, T.; Nohira, T.; Hagiwara, R. Polymorphism of Alkali Bis(fluorosulfonyl)amides (M[$N(SO_2F)_2$], M = Na, K, and Cs). *Inorg. Chem.* **2013**, *52*, 568−576.
(58) Mochida, T.; Funasako, Y.; Inagaki, T.; Li, M.-J.; Asahara, K.; Kuwahara, D. Crystal Structures and Phase-Transition Dynamics of Cobaltocenium Salts with Bis(perfluoroalkylsulfonyl)amide Anions: Remarkable Odd-Even Effect of the Fluorocarbon Chains in the Anion. *Chem. −Eur. J.* **2013**, *19*, 6257−6264.
(59) Sumitani, R.; Mochida, T. Thermal Properties, Crystal Structures, and Photoreactivity of Ru-Containing Ionic Liquids with Sulfur-Containing Substituents. *J. Mol. Liq.* **2021**, *344*, No. 117784.
(60) de Bruin, B.; Brands, J. A.; Donners, J. J. J. M.; Donners, M. P. J.; de Gelder, R.; Smits, J. M. M.; Gal, A. W.; Spek, A. L. Selective Oxidation of [Rh^{I}(cod)]$^{+}$ by H_2O_2 and O_2. *Chem. −Eur. J.* **1999**, *5*, 2921−2936.
(61) de Bruin, B.; Boerakker, M. J.; Donners, J. J. J. M.; Christiaans, B. E. C.; Schlebos, P. P. J.; de Gelder, R.; Smits, J. M. M.; Spek, A. L.; Gal, A. W. Oxidation of Rh^{I}(olefin) Fragments to 2-Rhoda(III)-Oxetanes. *Angew. Chem., Int. Ed.* **1997**, *36*, 2064−2067.
(62) Fernandez-Bartolome, E.; Martinez-Martinez, A.; Resines-Urien, E.; Piñeiro-Lopez, L.; Costa, J. S. Reversible Single-Crystal-to-Single-Crystal Transformations in Coordination Compounds Induced by External Stimuli. *Coord. Chem. Rev.* **2022**, *452*, No. 214281.
(63) Braga, D.; Maini, L.; Grepioni, F. Mechanochemical Preparation of Co-Crystals. *Chem. Soc. Rev.* **2013**, *42*, 7638−7648.
(64) Green, M.; Kuc, T. A.; Taylor, S. H. The Synthesis and Some Reactions of Bis(acetonitrile)(diene)-Rhodium and -Iridium Tetrafluoroborate. *J. Chem. Soc., Dalton Trans.* **1970**, 1553−1554.
(65) Tiripicchio, A.; Camellini, M. T.; Claver, C.; Ruiz, A.; Oro, L. A. Diolefin Cationic Rhodium Complexes with Sulfur Donors. X-Ray Structure of [$Rh(NBD)_2(SEt_2)$]ClO_4. *J. Organomet. Chem.* **1983**, *241*, 77−86.
(66) Dorta, R.; Rozenberg, H.; Shimon, L. J. W.; Milstein, D. Dimethylsulfoxide as a Ligand for Rh^{I} and Ir^{I} Complexes—Isolation, Structure, and Reactivity towards X-H Bonds (X = H, OH, OCH_3). *Chem.−Eur. J.* **2003**, *9*, 5237−5249.
(67) Bats, J. W.; Rivas Nass, A.; Hashmi, A. S. K. Low-Temperature Phase of Diaqua(1,5-cyclooctadiene)rhodium(I) Trifluoromethanesulfonate. *Acta Crystallogr., Sect. E: Struct. Rep. Online* **2004**, *60*, 85−87.
(68) Schenck, T. G.; Downes, J. M.; Milne, C. R. C.; Mackenzie, P. B.; Boucher, T. G.; Whelan, J.; Bosnich, B. Bimetallic Reactivity. Synthesis of Bimetallic Complexes Containing a Bis(phosphino)-pyrazole Ligand. *Inorg. Chem.* **1985**, *24*, 2334−2337.
(69) Shelly, K.; Finster, D. C.; Lee, Y. J.; Scheidt, W. R.; Reed, C. A. η^{1}-Benzene Coordination: The Synthesis and X-Ray Crystal Structure of a Novel Silver Salt of the Weakly Coordinating Carborane Anion $B_{11}CH_{12}^{-}$. *J. Am. Chem. Soc.* **1985**, *107*, 5955−5959.
(70) Davis, J. H.; Jeffrey, K. R.; Bloom, M.; Valic, M. I.; Higgs, T. P. Quadrupolar Echo Deuteron Magnetic Resonance Spectroscopy in Ordered Hydrocarbon Chains. *Chem. Phys. Lett.* **1976**, *42*, 390−394.
(71) Sheldrick, G. M. A Short History of SHELX. *Acta Crystallogr., Sect. A: Found. Crystallogr.* **2008**, *64*, 112−122.
(72) *APEX3, v2015.52*; Bruker AXS Inc.: Madison, WI, 2015.
(73) Macrae, C. F.; Bruno, I. J.; Chisholm, J. A.; Edgington, P. R.; McCabe, P.; Pidcock, E.; Rodriguez-Monge, L.; Taylor, R.; van de Streek, J.; Wood, P. A. Mercury CSD 2.0 − New Features for the Visualization and Investigation of Crystal Structures. *J. Appl. Crystallogr.* **2008**, *41*, 466−470.
(74) Spek, A. L. Structure Validation in Chemical Crystallography. *Acta Crystallogr., Sect. D: Biol. Crystallogr.* **2009**, *65*, 148−155.
(75) Sheldrick, G. M. *TWINABS v2012/1*; University of Göttingen, 2012.
(76) *XPREP v2014/2*; Bruker AXS Inc.: Madison, WI, 2014.

https://doi.org/10.1021/acs.inorgchem.2c03865
Inorg. Chem. 2023, 62, 2169−2180